2 PF-Ring

2-1 Summary

The upgrade project consisting of the extension of the ten existing straight sections and the creation of four new 1.4-m straight sections was successfully completed in FY2005. A new in-vacuum short gap undulator SGU#03 was installed in FY2006, and is described in the following section. Since a number of vacuum ducts were replaced during the project, the beam lifetime was reduced form to when the ring was re-operated, and it was necessary to inject electrons into the ring twice a day in multibunch mode until the end of 2006. The lifetime gradually recovered through routine operation, and injection frequency returned to the standard once-a-day in January 2007. The initial beam current of 450 mA in 2.5-GeV multibunch mode was unchanged throughout FY2006. The coupling impedance of the new vacuum duct was decreased, and consequently the bunch length in the higher single-bunch current was improved. The lifetime in the single-bunch operation was decreased by one-third following the upgrade, and six to eight injections were required per day.

The KEK linear accelerator switches the electron/positron beams to four storage rings: the KEKB HER(high-energy ring: 8-GeV e^-), the KEKB LER(low-energy ring: 3.5-GeV e^+), the PF(2.5-GeV e^-) and the PF-AR(3.0-GeV e^-). The fast switching project was launched in an effort to reduce the switching time between injection modes for these four rings which has been serious issues of the beam switching system, as described in the preceding volume. The fast switching system has been steadily developing and it will be possible to switch between the electron beams for the PF and for the KEKB HER within 20 ms. As part of this project, we began a top-up injection project for the PF ring, details of which are described in the following section. A test of top-up operation was performed during single-bunch user operation, maintaining the beam current at 50-mA. The result of this test showed that with the top-up injection a short lifetime becomes insignificant.

The history of ring operation time, scheduled user time and actual user time since 1982 is indicated in Fig. 2 of the preceding section. The annual operation schedule for FY2006 is indicated in Fig. 1 of the preceding section. The operation statistics of the PF ring for FY2006 are summarized in Table 1. The total operation time recovered from that of 2005, amounting to more than 5000 hours. Scheduled and actual user time excluding time losses due to machine troubles and daily injections were 4248 and 4160 hours, respectively. The ratio of actual user time to scheduled time has been maintained at 96-98% over the past 5 years. The trend of the product $I\tau$ of the beam current I and the beam lifetime τ over the past 10 years is indicated in Fig. 3. The small $I\tau$ after the upgrade in 2005 has gradually recovered as seen in Fig. 3. The $I\tau$ value dropped in the spring of 2006, as seen in Fig. 3. This was caused by a problem with the SR absorbers that is described in the following section. The change in the failure rate, which is defined as the failure time to the total operation time, is shown in Fig. 5. The failure rate was about 1% in the 1990s, and it has been reduced to about 0.5% over the past several years. However the failure rate increased to 0.85 % in FY2006. It is slightly larger than those in recent years due to the absorber trouble. In the FY2006, two one-week operations with 3-GeV multibunch mode, and also two one-week operations with 2.5-GeV single-bunch mode were performed. During 3-GeV operation, the beam current was limited to 200 mA because of the limitation on the RF power.

Table 1 Operation statistics of PF in FY2006.

	Multi-bunch	Single-bunch	Total
Ring Operation Time (hours)	4840.0	432.0	5272.0
Scheduled user time (hours)	3816.0	432.0	4248.0
Actual user time T (hours)	3743.3	416.7	4160.0
Time used for injection (hours)	32.4	10.2	42.6
Integrated current in T (A×hours)	1347.4	17.7	1365.1
Average current in T (mA)	360.0	42.5	--
Number of injections	285	88	373
Interval between injections (hours)	13.1	4.7	--

Timetable of the Machine Operation in FY 2006

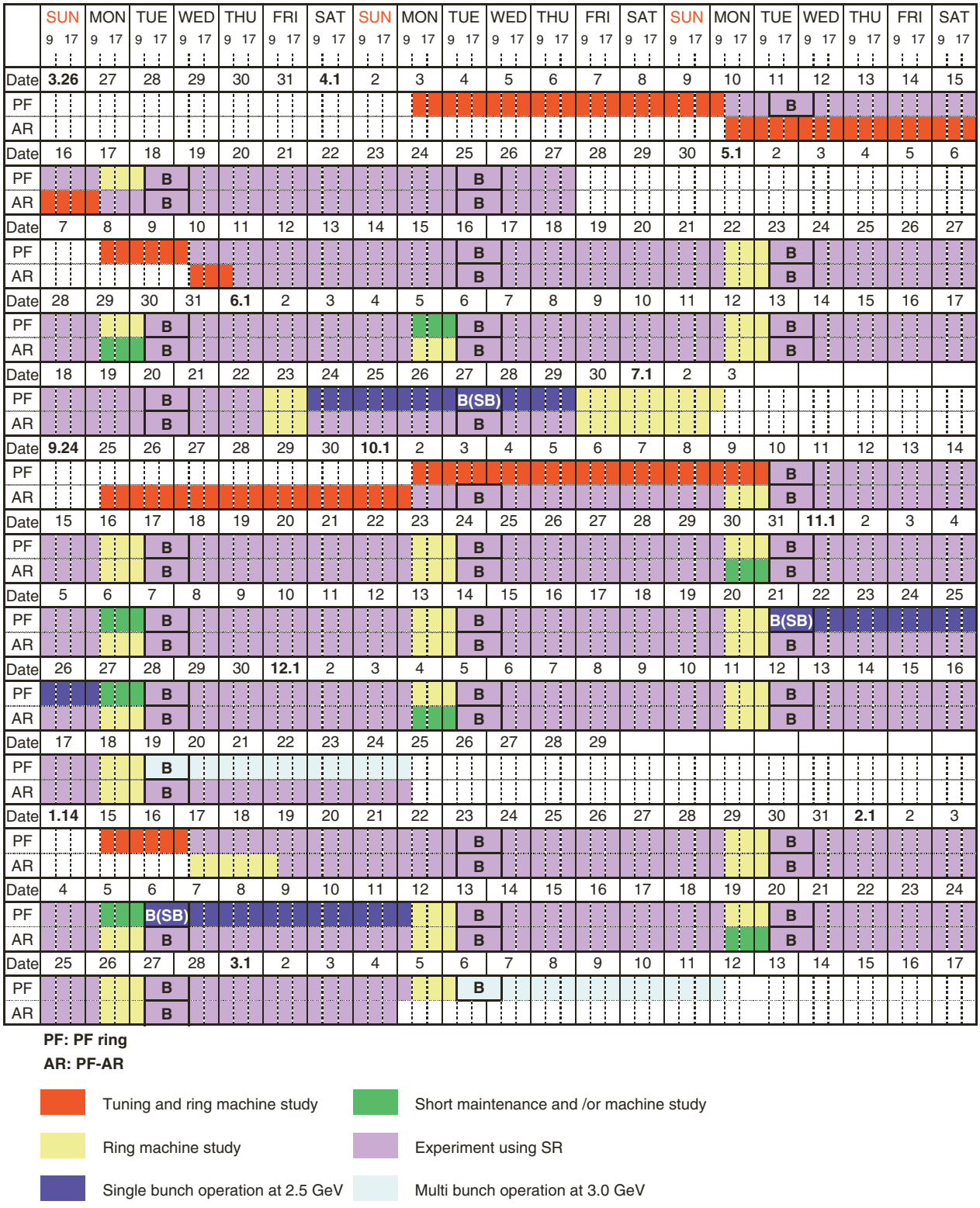

Figure 1
Timetable of machine operation in FY2006.

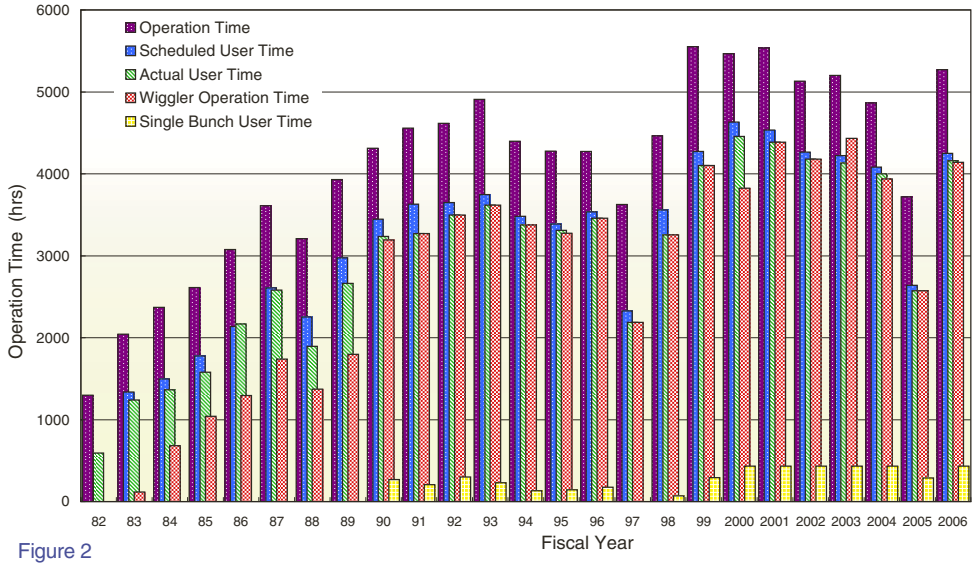

Figure 2
Operation time history of the PF Storage Ring.

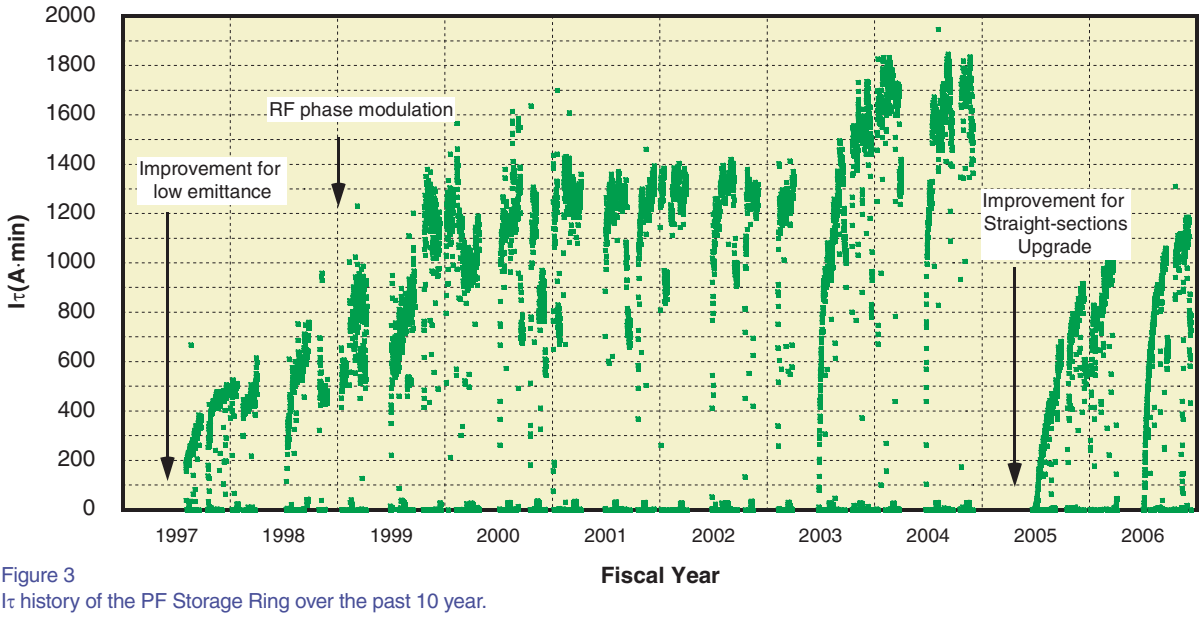

Figure 3
Iτ history of the PF Storage Ring over the past 10 year.

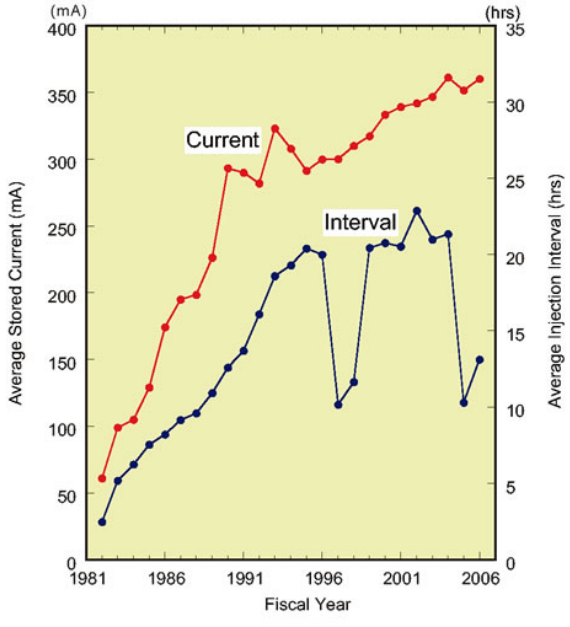

Figure 4
Average stored current and injection interval since 1982.

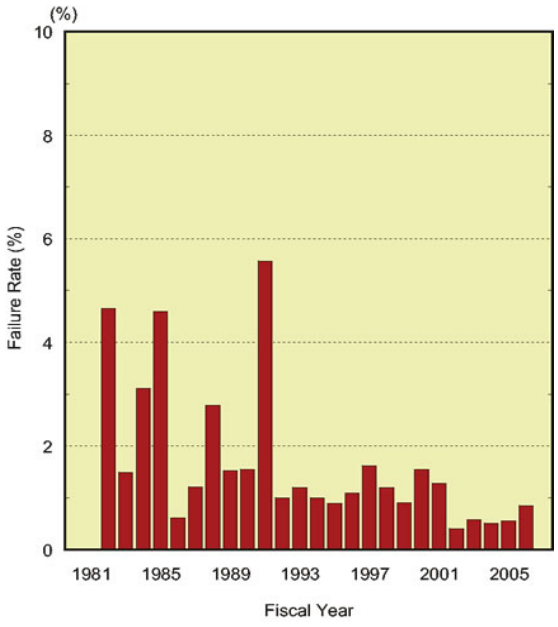

Figure 5
Failure rate history.

2-2 Vacuum Troubles of the Synchrotron Radiation Absorbers

At the beginning of the FY2006, vacuum leaks in the synchrotron radiation (SR) absorbers occurred in succession twice within one month. At the PF ring, most of the beam ducts are made of aluminum alloy, with a cooling-water channel is prepared on the extruded aluminum duct to act as a distributed absorber. In order to protect various devices including the RF-shielded bellows, many discrete OFHC copper absorbers are also installed along with the crotch absorbers. The leaks occurred two same model of these OFHC absorbers.

A cutaway viewing of the problem absorber is shown in Fig. 6. The absorber has a coaxial structure consisting of two copper tubes. The outer diameter is 10 mm with a sidewall thickness of 1 mm. The inner tube which provides the entrance for the cooling-water, has an outer diameter of 6 mm and a wall thickness of 1 mm.

Since no noticeable damage was found on the surfaces irradiated by the synchrotron radiation, the cause of the leak was investigated by cutting open one of the absorbers. The part of the water-cooling tube where the SR passes through was found to be remarkably eroded, and it was recognized that is where the vacuum leak occurred. The eroded area is labeled 1 in Fig. 6, and the erosion can be seen as a black pit in the photograph as shown in Fig. 7. Similar traces of erosion were found where the SR penetrated, on the inner pipe (labeled 2 in Fig. 6), and the other at the opposite side of the outer cylinder (labeled 3), a photograph of which is shown in Fig. 8.

This type of cooling pass erosion generated by the SR has already observed at the higher energy SR sources such as the ESRF and the SPring8. The vacuum leak from the crotch absorber was reported at the ESRF storage ring. It was recognized that we cannot ignore the SR promoted erosion even at the medium energy ring such as the PF ring. The absorbers at which the leaks appeared were installed during the large-scaled reconstruction of the PF ring in 1997, with eight and a half years passing until the first leak occurred.

A phenomenon regarded as erosion-corrosion was observed on the inner surface area labeled 4 and 5 in Fig. 6. The pipe wall has obviously thinned at certain locations, and ripple marks which was characteristic of erosion-corrosion were found on the inner surface, as can be seen in the Figs. 7 and 8. It is supposed that the velocity of the cooling-water was too fast for the copper tube, and that corrosion advanced by the water jet from the inner tube. This erosion-corrosion effect combined with SR promoted erosion to decrease the durability of the absorbers.

There are installed 28 similar absorbers in the PF ring, of which 24 were replaced during the summer shutdown of FY2006, with replacement of the remaining 4 carried over to the next fiscal year. The problem absorbers had an exceptionally small outer diameter because of the small setting space. The absorbers were incorporated in the standard ICF flanges at the end of stainless-steel duct. This coaxial structure is unfavorable from the view point of erosion-corrosion, and the wall thickness of 1 mm was also too thin. The replacement absorbers are made from dispersion strengthened copper, GlidCop, with a wall thickness of at least 3 mm and outer diameters as large as possible in the limited space. Situations where the SR passes through the cooling-water are avoided as much as possible.

During the first half year of operation following the upgrade project in FY2005, the product $I\tau$ of the beam current I and the beam lifetime τ had recovered to nearly 1000 A min at the beginning of FY2006 when the absorber leaks occurred. As a result of absorber replacement, the product $I\tau$ decreased temporarily after the summer shutdown, but was restored to about 1200 A min by the end of FY2006.

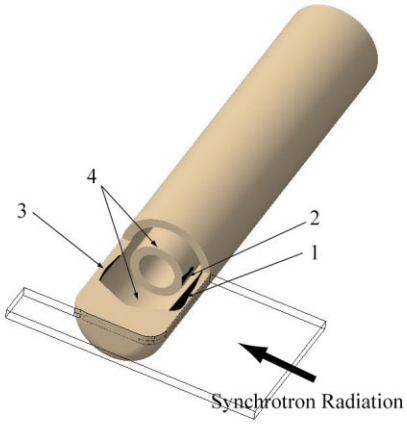

Figure 6
Cutaway viewing of the SR absorber which caused a vacuum leak.

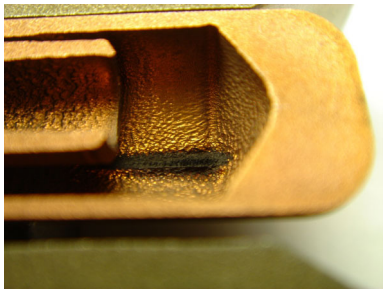

Figure 7
Photograph of the inner surface around the SR promoted erosion marked 1 in Fig. 6.

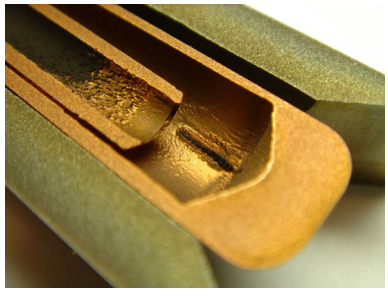

Figure 8
Photograph of the other side around the SR promoted erosion marked 3 in Fig. 6.

2-3 PF Top-up Injection

1. Injector upgrade for PF top-up

The KEK injector linac provides the beams with different modes sequentially for four storage rings; the KEKB Low Energy Ring (LER) (3.5-GeV e^+), the KEKB High Energy Ring (HER) (8-GeV e^-), Photon Factory ring (PF; 2.5-GeV e^-) and the Advanced Ring for pulse X-rays (PF-AR; 3-GeV e^-). The PF and PF-AR rings are injected once and twice daily, respectively. On the other hand, the KEKB rings are operated under the continuous injection in order to keep the stored current almost constant. To achieve top-up operation in the PF ring, the injector upgrade is strongly required so that one beam injection mode does not interrupt the beam injections for the other rings.

For each beam injection mode, the linac parameters should be changed since the required beam energy and charge is different for each mode. The main parameters include those of magnet power supplies, timing, rf phase and so on. Typically, the change of parameters takes a half-minute between KEKB e^- and e^+ modes, one minute between KEKB and PF modes. The final purpose of this upgrade is achieve switching of the linac parameters for each ring injection in less than 20 msec since the maximum linac beam repetition is 50 Hz. For this purpose, we are developing a "multi-energy linac scheme" in which magnet setting common to the KEKB and PF rings are used. The fast change of beam energy is achieved by rapidly changing the low-level RF phases. Although the PF ring use 2.5-GeV e^-, the beam is one time accelerated up to 5 GeV, then the beam will be decelerated to 2.5 GeV by using the deceleration phases. This method is effective for enlarging the common optics region. A machine study of the multi-energy linac scheme has shown that the beam size and emittance are almost the same as daily operation. We have also confirmed that the beam injection rates for the PF and KEKB e^- rings are high enough under the new scheme, and conclude that the scheme is feasible for realistic beam operation.

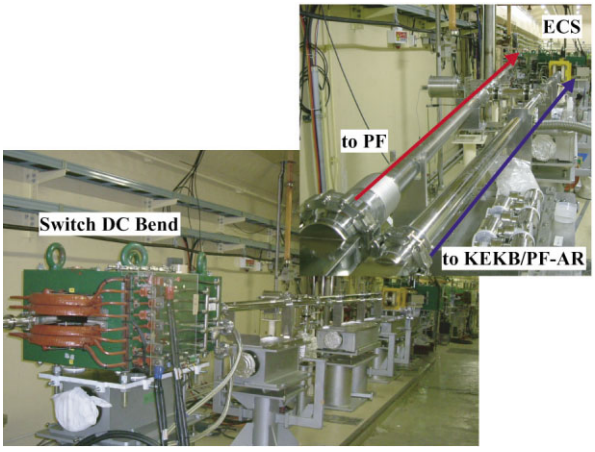

Figure 9
Photograph of switch DC bend for the new PF-BT (Phase-I).

2. Pulsed bend system

The injector upgrade will be performed in three phases, and in the phase-I, we have constructed a new PF-BT line in order to shorten the beam-mode switch between the KEKB and PF modes. A photograph of the switch DC bend for the new PF-BT is shown in Fig. 9. The former switch bend was placed downstream of the ECS magnets. In order to bypass the ECS, a new DC switch bend has been installed in the last stage of the linac by removing one accelerating unit. A new 60 m long PF-BT line was constructed in the summer of 2005. With this new PF-BT, there is no need to change the ECS parameter for switching between the KEKB and PF modes, and the total time required for switching from KEKB injection to PF injection and back again, including PF injection has been decreased from 5 min to 2.5 min. With optimization of the new PF-BT, the beam injection efficiency has increased by more than 30%. The radiation dose due to the beam losses has also been decreased.

In the phase-II, we aim to carry out the fast beam-mode switching between the KEKB e^- and PF modes by using the multi-energy linac scheme. The DC switch bend will be replaced by a new pulsed bend in the summer of 2007. The pulsed switch bending magnet system consists of a bending magnet, power supply and a ceramic chamber has been developed by the KEKB-BT group. Photographs of the pulsed-bending magnet and the pulsed-power supply are shown in Fig. 10 and Fig. 11 respectively. The parameters of pulse bending magnet system are given in Table 2. The required bending angle is 7 deg., and the maximum repetition rate is 25 Hz. The pulsed bend system was designed also to take care of future 3-GeV injection for the PF ring. The pulse shape of the magnet is a half-sine pulse with a peak current of 32 kA and a pulse length of 200 μs. The stability was better than 0.1%, in the test operations. The ceramic chamber will be also installed in the summer of 2007. To avoid due to heat load, the surface of the ceramic will be covered with a titanium nitride thin coating.

Table 2 Main parameters for pulsed bend system.

Power Supply	
Peak current	32 [kA]
Pulse width	200 [μs]
Stability	< 0.1%
Max. repetition	< 0.1%
Bend	
Turn	1 [turn]
Core length	0.99 [m]
Gap height	30 [mm]
Max. magnetic field	1.22 [T]
Magnetic field uniformity	$< 5\times10^{-3}$
Bending angle	7 [deg.]
Ceramic chamber	
Length	1200 [mm]
Coating materia	Ti
Coating depth	< 50 [nm]

3. Fast switching between e^- and e^+ modes

Phase-III will extend the fast beam-mode switching to e^+ beam operation. Currently switching on and off of the e^+ production target is mechanical. We will use an e^+ production target with a hole in side for the fast e^-/e^+ mode switch. When the beam of electrons is required, the trajectory of the primary e^- beam will be directed through the hole on the e^+ target. For a feasibility study, a new e^+ production target was installed. A picture of the target is shown in Fig.12. The target core is the crystalline-tungsten of diameter 5 mm. The hole is located 4.5 mm from the center of the tungsten target, and the diameter of the hole is 3 mm. Machine study results show that around 95% of the e^- beam passes through the hole compared to normal operation (e^+ target removed). The feasibility of this scheme thus seems confirmed, although more studies are required.

4. Status of the PF ring

During FY2006, we managed radiation safety issue for the top-up operation of PF ring. Many machine studies were performed for top-up injection. The most important progress in 2006 was top-up test operation in user time. During November 2006, the PF ring was injected keeping the beam shutter open, and in the first week of February 2007, a top-up test operation was successfully performed during single-bunch user operation.

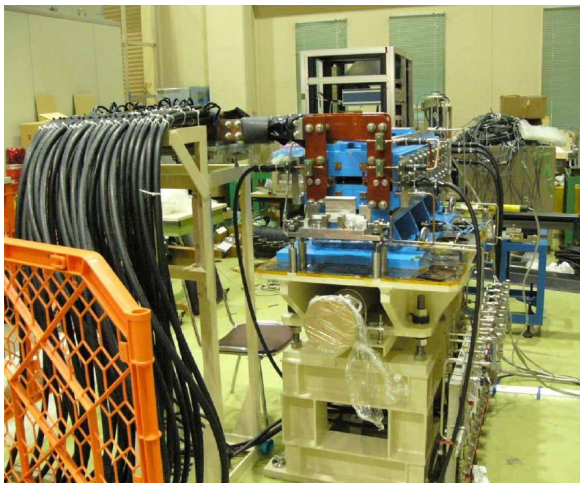

Figure 10
Photograph of pulsed bend.

Figure 11
Photograph of pulsed power supply.

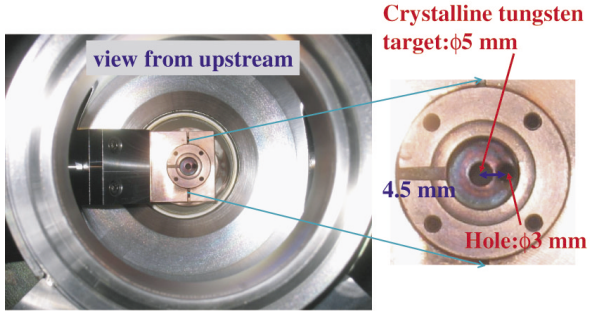

Figure 12
Photograph of e^+ production target for fast e^-/e^+ switch.

5. Radiation safety for top-up injection

For top-up operation, the beam power conditions for injection are set as follows;

1. The maximum power of the PF beam transport line is limited to 65 W. This power will be monitored by a wall-current monitor.
2. A new beam dump will be installed at the end of the PF beam transport line.
3. The beam power for the injection of PF ring will be limited to 6.6 W.
4. The beam power for top-up injection will be limited to 0.65 W.

A beam slit will be installed at the end of the beam transport line, and beam power regulated by varying the slit width.

To maintain radiation safety, we added following modes;

1. Injection mode

Injection of the PF ring from 0 mA to 450 mA with a 6.5 W beam.

During this mode, the main beam shutters of the SR beamlines must be closed.

2. Top-up injection mode

A stored beam of more than 10 mA is necessary for this mode.

The existence of a stored beam in the ring guarantees that the conditions (such as magnets and RF) are ready for the injection.

The beam transport slit must be set to satisfy condition 4 above.

All the radiation interlocks must be in a green state.

6. Machine studies for the top-up injection

During FY2006, the following machine studies were performed.

1. Optimization of the kicker magnets for the injection to reduce the oscillation of the stored beam.
2. Injection test by the use of a common configuration of the lattice for the PF and the B-factory.
3. Test of top-up injection test for both multi-bunch and single bunch operations.
4. Aperture survey for top-up injection with a vertical scraper.

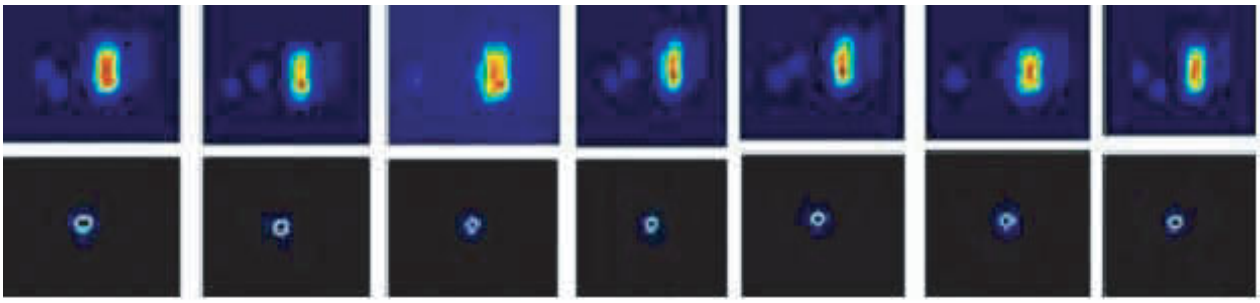

Figure 13
A comparison of the oscillation of the stored beam observed during study in 2006 (lower row) with previous results from 2005 (upper row).

The results of these studies are described in the following subsections.

1) Optimization of the kicker magnets to reduce oscillation of the stored beam.

Investigations have been performed to optimize the injection kicker magnets to compensate for the oscillation of the stored beam. A comparison of the oscillation of the stored beam observed during this study with previous results from 2005 is shown in Fig. 13. In FY2006, we realigned the quadrupole magnets of the ring. The optimization of the kicker combined with this realignment have almost removed the vertical oscillation of the beam which was observed in 2005. The remaining oscillation in the horizontal direction is amounts to less than 1/3 of the horizontal beam size.

2) Injection test by the use of a common configuration of the lattice for both of the PF and the B-factory of the linac.

Injection by using a common configuration of the lattice for the PF and the B-factory of the linac is necessary to allow top-up operation of the PF ring during the operation of the B-factory. We have designed a common lattice configuration for injecting both of a 2.5 GeV beam for the PF and a 8-GeV beam for the B-factory. For the PF ring, the electron beam is accelerated to 5 GeV in the first three sectors of the linac, and decelerated to 2.5 GeV by the later sectors (sectors 4 and 5). To match the lattice of the PF beam transport line to the common lattice configuration, we have established an injection speed of 1.5 mA/sec, which is almost same for the normal PF injection.

3) Test of top-up injection for both multi-bunch and single bunch operations.

On 16th January 2006, we tested top-up injection for both multi-bunch and single bunch operations. A plot of the ring current during the multi-bunch top-up test is shown in Fig. 14. At the beginning of the study, the beam was injected into the PF ring continuously, and the radiation dose monitored. Following the radiation survey, the beam power was limited using the beam transport slit to maintain an injection speed of 0.1 mA/sec with an injection repetition of 1 Hz. The beam was ON/OFF controlled by the beam gate to keep the ring current constant at 450 mA. Similar tests were performed for single bunch-operation at the ring currents of 41 mA, 51 mA and 60 mA. A plot of the ring current during single-bunch top-up test is shown in Fig 15. We were successful in keeping ring current fluctuations to less than ±0.1 mA during all the tests.

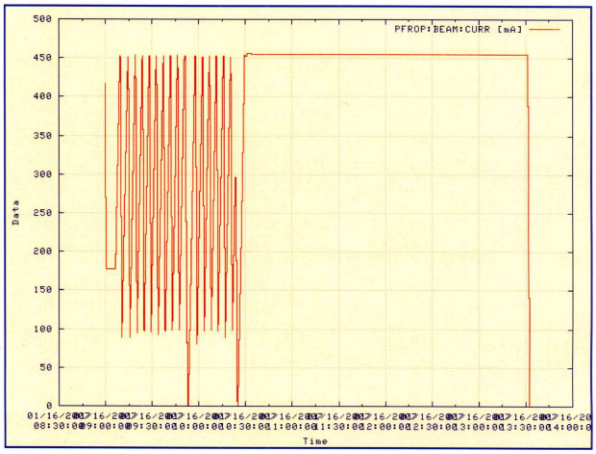

Figure 14
A plot of the ring current during the multi-bunch top-up test.

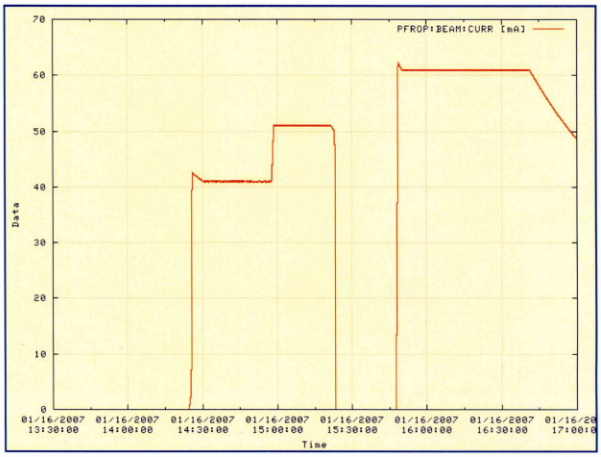

Figure 15
A plot of the ring current during single-bunch top-up test.

4) Aperture survey for top-up injection with a vertical scraper.

It is very important to confirm that it is possible to inject the beam with the narrow aperture presented by the insertion devices. To estimate the injection aperture, we used a scraper which is set in the straight section between the bending magnets 4 and 5. The aperture survey shows that a 10-mm aperture at the scraper was necessary for injection. Scaling the β -function, this corresponds to 3.3-mm at the short-gap undulators. The minimum gap of the short-gap undulators is 4-mm, so that injection beam can pass through. During actual top-up operation, we will use the slit at the end of the beam transport line to limit the injection beam size.

In addition to the above mentioned studies, many more machine studies were performed, including studying a feedback system to stabilize beam instabilities. Details of the feedback system is described elsewhere in this pp106.

7. Test operation of top-up injection mode during single bunch user operation

A test operation of normal injection with open main beam shutters (MBS) was performed during the single-bunch user operation of the forth week of November 2006. In first week of February 2007, a top-up test operation was performed during single-bunch user operation. In the top-up test operation, the injection speed was regulated to be almost the same as the decay speed (0.01 mA/sec) with an injection repetition of 1 Hz. The operation pattern is repeating sequence of 10 sec injection and 10 sec storage. The beam was ON/OFF controlled by the beam gate to keep a constant ring current of 50 mA. The typical operation pattern is shown in Fig. 16. The ring current is seen to be stabilized at 51±0.08 mA. A typical one-day history of the ring current is given in Fig. 17, which also shows tow drops in current due to injection of the PF-AR ring. The scheduled and accidental interruptions during the week-long top-up test operation are summarized as follows;

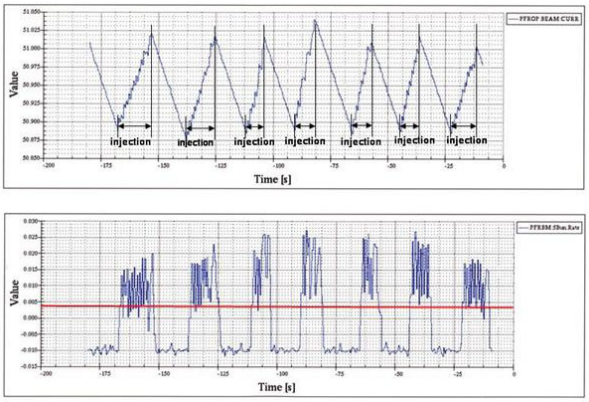

Figure 16
Typical operation pattern of the top-up operation.

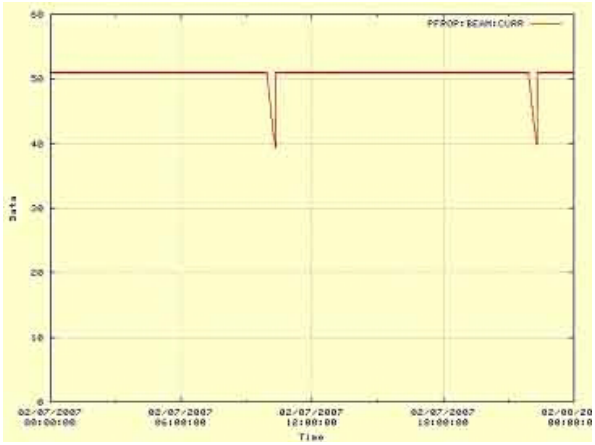

Figure 17
Typical one-day history of ring current in the top-up operation.

1. Scheduled interruptions
   - PF-AR injection — twice daily
   - Linac maintenance — 1 shift (8 hours) every 2 weeks
2. Accidental interruptions
   - Irregular injection for the PF-AR — twice
   - Linac Klystron fault — 12 times
   - Miss operation linac interlock door — once

Linac Klystron faults are normally recovered from in less than several ten second. But the current drops were very small and not significant. During the 8 hours linac maintenance period, the PF ring was operated in the normal storage mode.

8. Schedule

As mentioned in the Licac schedule, a pulse-bending magnet for switching the beam to the PF ring will be installed in the summer shut down of 2007. Following this installation, it will be possible to test the fast switching mode of the multi-energy Linac scheme. Once successful operation of this scheme has been establishment, t will be used to inject the PF ring. Following a successful short-term test (one week) of top-up operation, we plan to perform long-term (few months) test operations in 2008 to check stability. At present it is only possible to operate the PF ring in top-up mode when the B-factory is operating in electron mode, since the electron beam is not available when the B-factory is being injected with positrons. Since as mentioned in above, test on the special target which has a hole in the side to allow electron beam acceleration even during the positron operation mode will start in autumn 2007, so it is expected that it will be possible to operate the PF ring with full-time top-up injection in the near future.

2-4 Research and Development

1. Construction and Commissioning of the SGU#03 Short-gap Undulator

The Photon Factory straight-sections upgrade project was completed in 2005, and details of the upgrade have been reported elsewhere[1]. During the upgrade, four new 1.4-m straight sections were created, and the lengths of the existing ones were nearly doubled. The new 1.4-m straight sections are designed to have small betatron functions, to allow the installation of in-vacuum undulators with very short magnetic periods and gaps.

Even with the 2.5-GeV beam energy of the PF ring, it is possible to produce hard-rays with energies of up to 15 keV using the low (<7) harmonics if a very short period length is chosen for the undulator. However, this is only possible if the undulator gap can be closed down to 5 mm or less to obtain a high enough field strength. These two requirements can be met by a combination of in-vacuum undulator technology [2, 3] and advanced lattice design using small betatron functions [4].

For this purpose, we have developed short-period and small-gap undulators (SGU) in an in-vacuum configuration [5]. The first SGU, SGU#17, was installed in 2005 at one of the new 1.4-m straight sections, between bending magnets B#16 and B#17 in the upgraded PF lattice. The vertical betatron function is designed to be 0.4 m at the centers of the new straight sections to allow for a minimum gap of 4.5 mm for the SGUs. In 2006 a second SGU, SGU#03, was constructed and installed in the new 1.4-m straight section located between bending magnets B#02 and B#03. This SGU will be dedicated to the research field of solid state physics.

The magnetic and mechanical structures of SGU#03 are very similar to those of SGU#17. A pure Halbach magnet arrangement with a period length (λ_u) of 18 mm and a periodicity (*N*) of 26 was chosen. For the magnet material we have selected Nd-Fe-B alloy with a remanent field of *Br*=12.0 kG and coercivity *iHc*=28.0 kOe (NEOMAX35VH manufactured by NEOMAX Co. Ltd.). This material offers excellent magnetic performance and endurance against high temperatures for baking. The magnet blocks are coated with TiN (5 μm thick) for vacuum sealing, embedded in an oxygen-free copper holder, and attached to a pair of Al alloy magnet-mounting beams.

The internal surfaces of the 980 mm long, 250 mm inner diameter stainless steel vacuum chamber were electrolytically polished, and the chamber is evacuated using a combination of Ti sublimation (TSP) pumps and sputter ion (SIP) pumps. A pressure of 7.5×10^{-10} Torr can be reached following baking at 120°C for 48 hrs. The magnet gap can be varied from 40 mm to 4.5 mm (with the deflection parameter *K* ranging up to 1.54). The gap width is controlled by a translation system composed of precise ball screws and linear guides. Translation is transmitted to the magnet arrays by linear motion feedthroughs using bellows couplings. In order to avoid problems due to Ohmic and parasitic mode losses, the opposing faces of the magnet arrays are covered with thin metal foils. This foil (60 μm thick) made of oxygen-free copper is plated with Ni (25 μm thick) for magnetic sustainment of this foil on the magnet face. We also put a contactor composed of a foil of Be-Cu (180 μm thick), which flexibly connects the end of the magnet array to the *Q* duct of the PF ring. This type of flexible contactor originates from the in-vacuum undulator, U#NE3 which was installed in the 6.5 GeV PF-AR [2]. In order to prevent problems due to Ohmic losses at this contactor when the SGU is set to the very short gap of the order of 5 mm or less, we put a water-cooling pipe to a base block of the contactor. Heat due to Ohmic losses by the image current in the contactor will be removed by heat conduction through this block which is made of oxygen-free copper.

Field adjustments were made on the basis of precise field measurements. For this purpose, we have devised a new magnetic detector using Hall probes which are oriented in the *y*- and *x*- directions as shown in Fig. 19. The sensor part of the detector is designed to fit into a very small gap as small as 3 mm, and is a kind

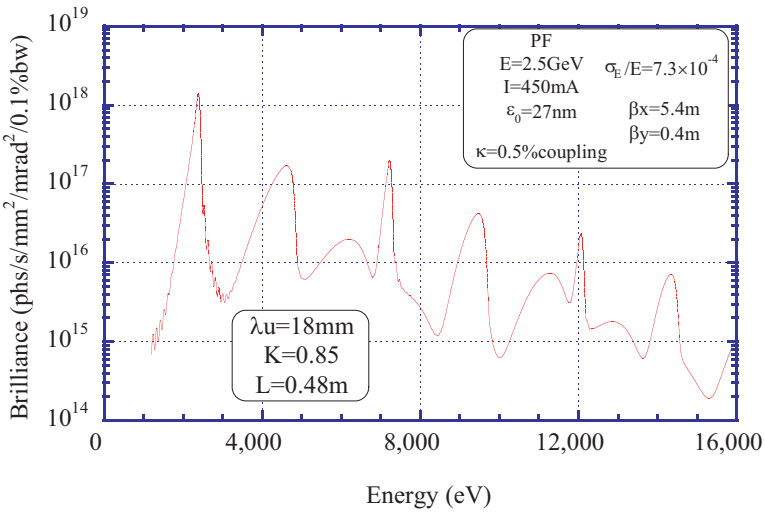

Figure 18
Calculated spectrum of the radiation from SGU#03 (λ_u = 18 mm) at the PF ring, for *K* = 0.85, and the ring parameters given in the figure.

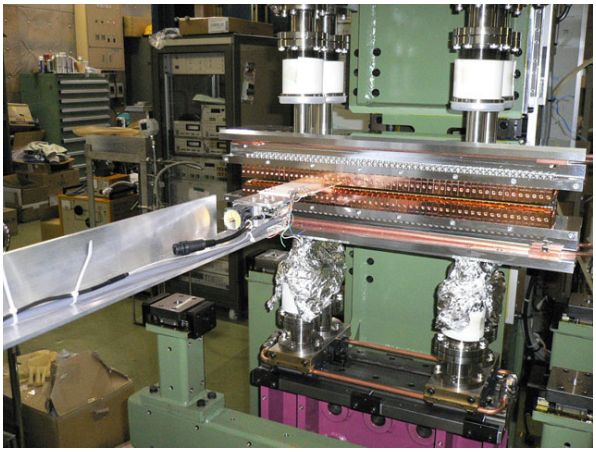

Figure 19
SGU#03 magnets undergoing field adjustment.

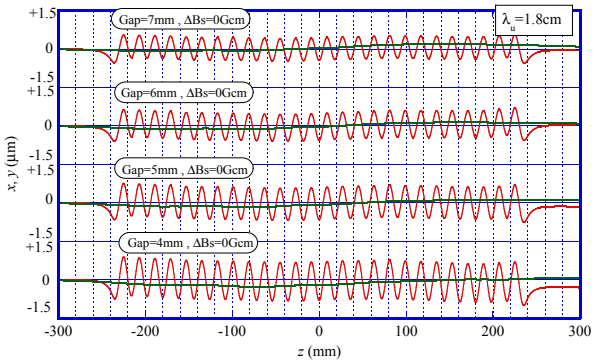

Figure 20
Summary of the field adjustment of SGU#03 (λ_u=18 mm). x (horizontal) and y (vertical) orbits are shown at several gaps. ΔB_S, denoting the field integrals at the entrance part of SGU#03 are negligibly small.

of Cu micro-oven equipped with a thermistor-type thermometer and heaters. The detector temperature can be controlled to an accuracy of 0.01°C [6]. We have adjusted the undulator field by optimizing a kick angle of the electron at each pole finally to have an ideal sinusoidal orbit in the horizontal plane and also to have a straight orbit in the vertical plane. As an adjustment method, we employ: (1) exchange of the magnet blocks and (2) insertion of disk-shaped magnet chips into holders of the magnet blocks.

The electron orbits in the undulator are summarized in Fig. 20. The quality of the undulator fields is satisfactory throughout the whole range of gaps, even though field adjustment was performed only for a gap of 5 mm. We also have satisfactory results on the kicks at the undulator's entrance and exit that violate parallelism between the electron orbit and the undulator. We find that both the absolute values of the kicks and their relative changes are satisfactorily small. In Fig. 20 the kicks at the entrance are shown as a field integral ΔB_S (Gcm). The effects of field errors on each harmonic can be described by the ratio of the real brilliance of the radiation to the ideal case. The real brilliance is calculated in case of a single electron using measured field data, whereas the ideal brilliance is calculated for an error-

Figure 21
Installation of SGU#03.

free field. For SGU#03, the brilliance ratio is as high as 95% for the fifth harmonic as a result of the fine field adjustments. The field errors are also evaluated in terms of optical phase errors, and the root-mean-square error of the optical phase was found to be as small as 2.4 degrees.

SGU#03 was installed into the PF ring in June 2006 (Fig. 21). During commissioning it was found that a gap of 3.8 mm was allowable, narrower than the designed 4.5 mm. It was also found that the gap could be tuned independently without the need for orbit correction. The orbit difference in both the *x*- and *y*-directions is less than 5 μm throughout the whole ring when the gap decreases from the maximum 40 mm to 4 mm. Characterization of the radiation from SGU#03 is now underway.

References

[1] T. Honda, S. Asaoka, W.X. Cheng, K. Haga, K. Harada, Y. Hori, M. Izawa, T. Kasuga, Y. Kobayashi, H. Maezawa, A. Mishina, T. Mitsuhashi, T. Miyajima, H. Miyauchi, S. Nagahashi, T. Nogami, T. Obina, C.O. Pak, S. Sakanaka, H. Sasaki, Y. Sato, T. Shioya, M. Tadano, T. Takahashi, Y. Tanimoto, K. Tsuchiya, T. Uchiyama, A. Ueda, K. Umemori and S. Yamamoto, *AIP Conf. Proc.* **879** (2007) 87.

[2] S. Yamamoto, T. Shioya, M. Hara, H. Kitamura, X.W. Zhang, T. Mochizuki, H. Sugiyama and M. Ando, *Rev. Sci. Instrum.* **63** (1992) 400.

[3] S. Yamamoto, K. Tsuchiya and T. Shioya, *AIP Conf. Proc.* **705** (2004) 211.

[4] Y. Kobayashi, *Photon Factory Activity Report* **#20** (2002) 98.

[5] S. Yamamoto, K. Tsuchiya and T. Shioya, *AIP Conf. Proc.* **879** (2007) 384.

[6] S. Yamamoto, T. Shioya, H. Kitamura and K. Tsuchiya, *Rev. Sci. Instrum.* **66** (1995) 1996.

2. Longitudinal Feedback System

Longitudinal coupled-bunch instabilities are observed for multi-bunch beam currents above 50 mA. The source of these instabilities was thought to be the broad-band impedance caused by narrow or step structures in the vacuum ducts. During 2005, ring upgrade the straight sections were renovated. Old vacuum components such as RF-unshielded bellows were replaced by new ones with RF-shields. After the vacuum duct replacement, the threshold current for longitudinal instability increased from 50 mA to 63 mA. During user operation, a phase modulation on the RF accelerating frequency at twice the synchrotron frequency is applied for suppression of the longitudinal instabilities [1]. The energy spread of the beam was increased after applying this technique. This increase of energy spread enlarges the bunch volume, and consequently the beam lifetime was extended about the factor of 1.5.

A top-up injection project is under way at the PF. Since short beam lifetime is not significant during top-up operation, the longitudinal feedback system is strongly necessary to stabilize the longitudinal instabilities. A longitudinal kicker based on a DAΦNE-type cavity has been designed and constructed, with the number of input and output ports reduced from 4 to 2. A schematic drawing of the internal structure of longitudinal kicker is shown in Fig. 22(a). A photograph of the cavity installed downstream of the accelerating cavity is also shown in Fig. 22(b). The beam-induced wakefield and impedance of the cavity was simulated using the MAFIA code. The designed impedance of the cavity is 700 Ω. The result of the simulation predict the shortest growth time of instability excited by the cavity to be longer than radiation damping time. This result shows the cavity will not excite any new instabilities. The transmission parameter S21 was measured in order to investigate the characteristics of the cavity. From this measurement, the 3 dB bandwidth of the resonant frequency was found to be 150 MHz, compared to a design value of 250 MHz. This disagreement was found to be due to a difference of the dimensions of the ridge part of the cavity from the design values. Since the observed instability modes exist within 6 dB, this difference will not lead to serious problems, and it was decided to install the cavity into the PF-Ring during the summer of 2006.

An analog mode-feedback system to suppress an instability mode was constructed in order to test the cavity performance. One longitudinal coupled-bunch mode was observed in the beam spectrum at low beam current, and the frequency of the instability was identified to be 942.5 MHz (mode number = 275). The signals from two diagonal BPMs are summed to eliminate the effects of the transverse motion of the beam. A local oscillator, which locked to the main RF signal via 10 MHz external clock, is used to detect the instability mode. The detected synchrotron-oscillation signal at 24 kHz is amplified and shifted by 90 degrees by an analog phase shifter. The single side band (SSB) signal is necessary for the feedback. The IQ modulator, which consists of a local oscillator locked to a frequency of $2 \times f_{RF} + n \times f_{rev}$, is used to generate the SSB signal as shown in Fig. 23. The external 10-MHz signal is used to lock the main RF accelerating frequency. The output of the modulator is amplified by 500-W amplifiers (R&K, A0812-6057) and fed into the feedback cavity. A high power circulator is necessary to protect the amplifier from the reflections from the cavity, and to match the impedance between the cavity and the amplifier. Since this circulator was not available during the test described here, the power amplifier was directly connected to the cavity using 8-D coaxial cable.

The beam spectrum without feedback as measured using the button electrode is shown in Fig. 23(a). The center frequency of the spectrum analyzer was set to $2 \times f_{RF}$ (= 1 GHz), and the span was set to 1 GHz.

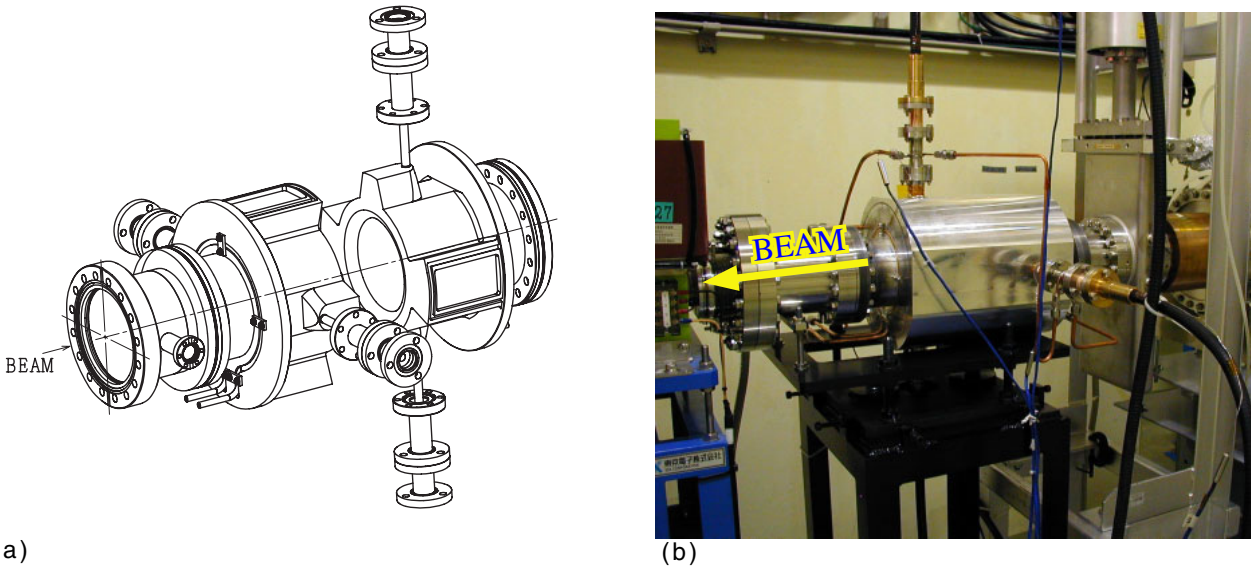

(a) (b)

Figure 22
Drawing (a) and a photo (b) of the longitudinal kicker installed at downstream of the RF accelerating cavity. The direction of the electron beam is also indicated in the figure. The blue cables seen in the photograph are temperature sensors.

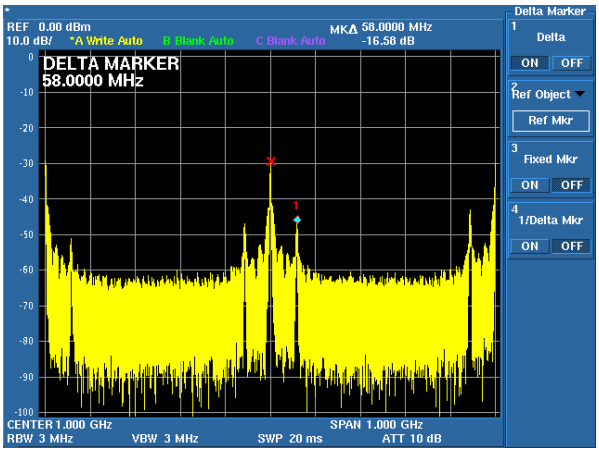

(a)

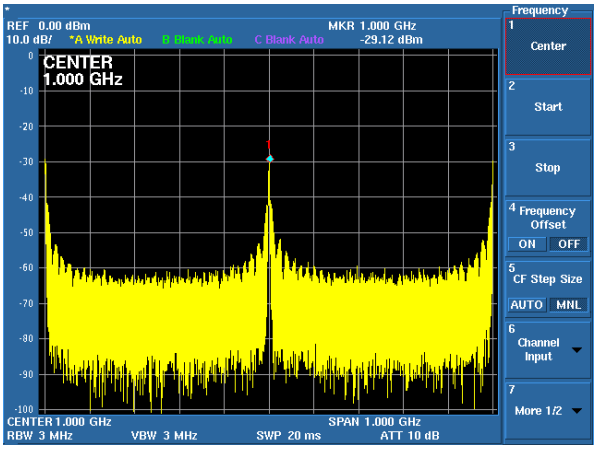

(b)

Figure 23
Beam spectrum measured using a button electrode with the feedback system turned off (a) and on (b).

The filling pattern of the storage ring was the same as for user operation with 280 buckets filled out of the harmonic number of 312. The tail around the RF harmonics arises from the filling pattern. The peaks in the tail are caused by the longitudinal coupled bunch instability, observed 58 MHz away from the RF harmonics. When the mode feedback loop is closed, these peaks in the spectrum disappear as shown in Fig. 23 (b). In this experiment, we successfully compensated for the instability for beam current of up to 70 mA. The high power circulator was not used during this experiment, and this current was limited by the reflection interlock of the power amplifier.

During actual operations, we will use a digital bunch-by-bunch feedback system. We plan to use a GBoard [3] developed by SLAC, KEKB, DAΦNE, and others for the signal processing. This system consisted of a 1 GSPS 8-bit analog-to-digital converter (ADC), Virtex-II FPGA and 12-bit digital-to-analog converter (DAC). For longitudinal feedback purposes, the synchrotron frequency is much slower than the bunch frequency. In the GBoard, a downsampling feature can be used to save the FPGA logic size. The high power circulator and the digital feedback system will be installed during FY2007.

References

[1] S. Sakanaka, M. Izawa, T. Mitsuhashi and T. Takahashi, *Phys. Rev. ST Accel. Beams* **3**, (2000) 050701.
[2] W.X. Cheng, T. Obina, T.Honda, M. Izawa, M. Tadano, M. Tobiyama, T. Nakamura and K. Kobayashil, *EPAC2006* (2006) 3009.
[3] D. Teytelman, R. Akre, J. Fox, A.K. Krasnykh, C.H. Rivetta, D.Van Winkle, A. Drago, J.W. Flanagan, T. Naito and M. Tobiyama, *EPAC2006* (2006) 3038.

3. Bunch Lengthening Effects in the Single-bunch Operation

The measurement of bunch shape and length during single-bunch operation plays an important role in revealing the interaction between the beam and its surroundings vacuum walls. When the beam current is low, the longitudinal bunch shape is observed to follow a Gaussian distribution. With increasing of the beam current, the bunch shape becomes asymmetric, with the tail of the distribution longer than the head. This phenomenon is caused by a potential well distortion induced by the resistive impedance of the vacuum components. For high beam currents, i.e., currents above the threshold current for microwave instability, the bunch shape is even more deformed from a Gaussian shape. Irregular bunch shape, and the changes in the bunch length are also observed.

A streak camera is a powerful tool for the instantaneous measurement of bunch shape and length. In conventional measurements, a monochromator, such as a band-pass filter, is used in order to reduce dispersion effects (e.g., chromatic aberrations) in the lens system. However, band-pass filters will reduce the intensity of the incident SR to less than 1/10, which often makes the bunch length difficult to measure for very low currents. In order to overcome this difficulty, we have designed and installed an optical relay system based on a reflective optics [1-2]. Newtonian-objective optics is employed to make an image of the beam profile onto the entrance slit of the streak camera. Since there is no monochromator intensity loss in the reflective optics, we can measure the bunch length for the beam current as low as 0.1 mA. The optical layout of the bunch lengthening measurement system is shown in Fig. 24. To reduce heat load from the hard X-ray components of the SR, a water-cooled beryllium mirror is used to reflect the visible light components of the SR. The distance from the source point to the streak camera is approximately 15 m.

Results of the bunch length measurements are shown in Fig. 25. The data points are the average of ten times measurements, with the error bars representing the minimum and maximum measurements. The theoretical natural-bunch length is also shown in the figure by a solid line. The theoretical value is in good agreement with the measurement for low beam current. For current below the threshold for microwave instability, we have attempted to estimate the potential well effect

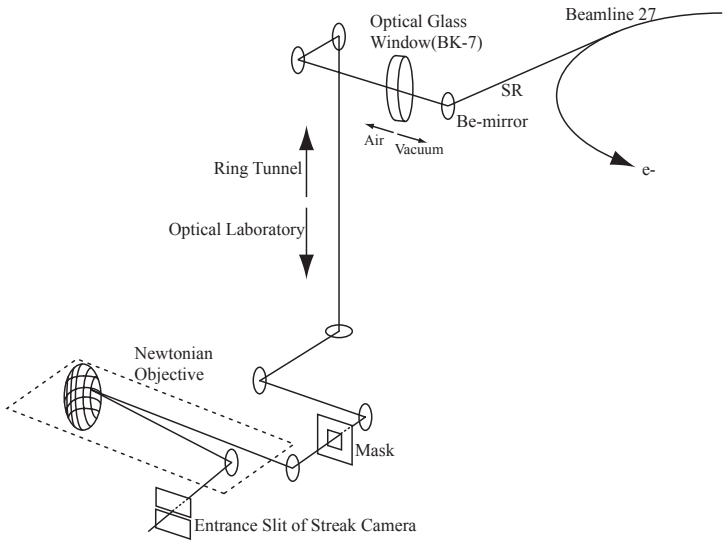

Figure 24
Optical layout of the bunch length measurement. The optical laboratory is located at the underground level of the storage ring.

using a classical model [3,4]. The results are shown in Fig. 26. The natural bunch length in the PF-Ring is approximately 22 mm FWHM, comparable to aperture of the vacuum duct (typically 38 mm in height and 90 mm in width).

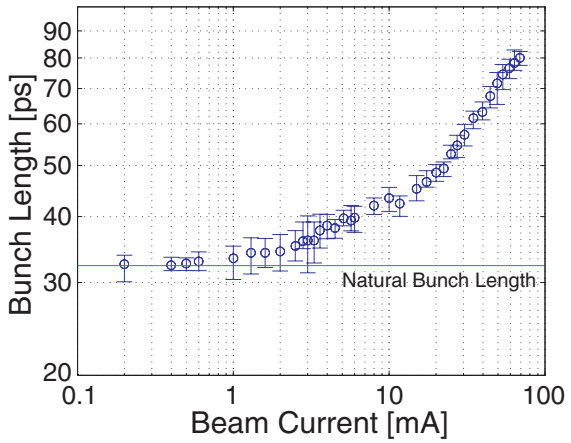

Figure 25
Bunch length measured by the reflective optics. The natural bunch length is also indicated in the figure.

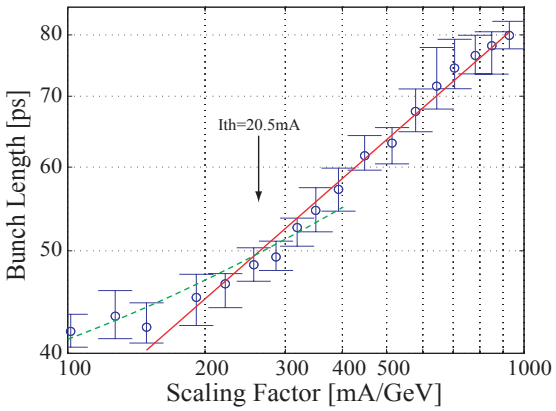

Figure 26
Bunch length above the threshold. The solid line and dotted lines denote the calculation using the scaling low and potential well distortion model, respectively.

Above the threshold current, the Chao-Gareyte scaling law holds, with the longitudinal broadband impedance depending on frequency with the form $z(\omega) \propto \omega^{a}$. The Chao-Gareyte scaling law, the bunch length is proportional to the power of the scaling parameter [5,6]:

$$\sigma \propto \xi^{1/(2+a)} = \left(\frac{\alpha I_b}{E \nu_{s0}^2} \right)^{1/(2+a)},$$

where I_b is the beam current, α denotes the momentum compaction factor and E the beam energy, ν_{s0} the unperturbed synchrotron tune, and ξ is a scaling parameter. The bunch length data was fitted to this scaling law for current above threshold, resulting in the solid line shown in Fig. 26.

From the potential well model and scaling estimation, the threshold current of microwave instability was determined to be 20.5 mA and the corresponding coupling impedance to be 0.5 Ω.

In March 2005, the upgraded project of the PF was successfully completed. The project aimed to introduce four new straight sections for the short-gap undulators and to lengthen the existing straight sections. Before the upgrade, the threshold current for microwave instability was 12 mA and the corresponding impedance was 1.1 Ω. After the upgrade, the threshold current has been improved because the old vacuum components such as RF-unshielded bellows and cavity-like structures have been cured. We also plan to measure a change in the energy spread in order to confirm the threshold current.

References

[1] T. Obina and T. Mitsuhashi, "Measurement of bunch lengthenigng effects using a streak camera with reflectiveoptics", to be published in *Proc. DIPAC 2007.*
[2] T. Mitsuhashi and M. Tadano, *PAC'03* (2003) 2506.
[3] B. Zotter, *CERN/ISR-TH* 78-16 (1978)16.
[4] T. Nakamura, *PAC'91* (1991) 440.
[5] A. Chao and J. Gareyte, *Particle Accelerators*, **25** (1990) 229.
[6] A. Hofmann and J.R. Maidment, *LEP note* **168** (1979).

4. Orbit switching Kicker system for the variably-polarlizing tandem undulators at BL-16

The user experiments with the 10-Hz light polarization switching are planned at the BL-16 of the PF ring. Two APPLE II type undulators and a bump orbit switching by kicker magnets system will be installed in order to realize the experiments. A conceptual design of the orbit switching system is shown in Fig. 27. The system consists of the five sets of same kicker magnets and power supplies. The magnet core is made by a lamination of the 0.5 mm thickness silicon steel. A drawing of the kicker magnet is shown in Fig. 28. The specifications are shown in Table 3. The capacity of the power supply is 5 kW (±50 V, ±100 A). A conceptual diagram of the system is shown in Fig. 29. For the orbit switching operations, the bump height is varied sinusoidally. In order to close the bump with the static magnetic errors and the insertion devices, it may be necessary to modulate the current waveforms of the kickers to provide the feed-forward correction. For the fast orbit feedback correction, the fast steering magnet and the local orbit measurement system will be installed. In order to avoid the attenuation and retardation of the magnetic field by the eddy current effect, the stainless steel of thickness 2 mm is used for the vacuum duct. The system was designed in 2006, and will be manufactured during 2007. The bump system with one insertion device will be installed in March, 2008, and initial orbit bump studies will be conducted with a single insertion device.

Table 3 Main parameters of the magnets.

Beam energy	E [GeV]	3.0
Kick angle	θ [mrad]	2.4
Magnetic field	B [T]	0.16
Vertical pole gap	h [mm]	16
Horizontal pole width	w [mm]	110
Magnet core length	l [mm]	150
Coil turn number	N [turns]	32
Inductance	L [H]	1.0×10^{-3}
Magnetic current	I [A]	83.5
Resistance	R [Ω]	0.1
Frequency	f [Hz]	10
Voltage	V [V]	13.7
Silicon steel thickness	t [mm]	0.5

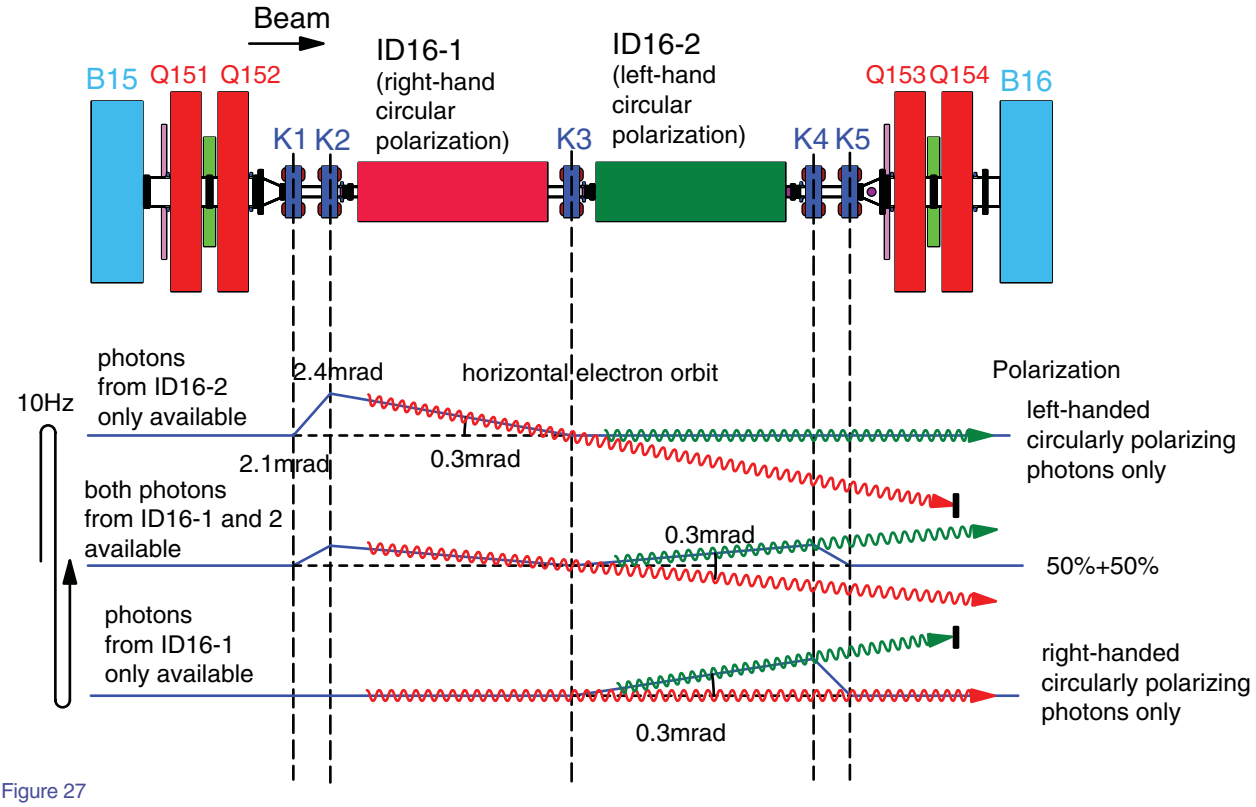

Figure 27
Concept of the orbit switching.

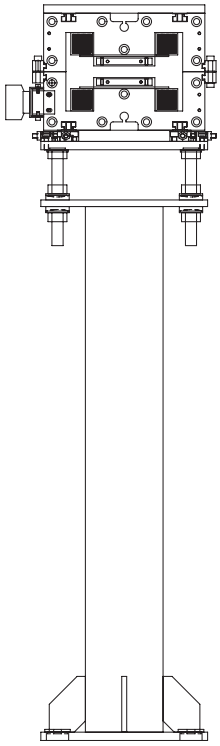

Figure 28
Bump magnet.

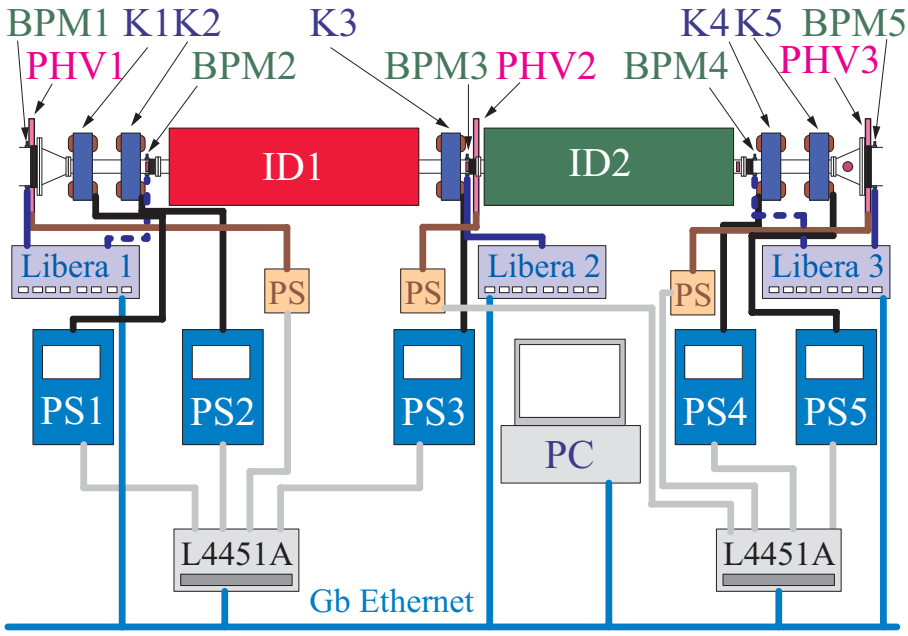

Figure 29
"K1" ~ "K5" are the bump magnets, "PS1" ~ "PS5" the power supplies, "BPM1" ~ "BPM5" the beam position monitors, and "PHV1" ~ "PHV3" the fast steering magnets. The signal processors for the BPMs are shown as "Libera1" ~ "Libera3". The currents of the kicker and the steering magnets are set by a 4-channel ADC (analog-to-digital converter) shown as "L4451A". "PC" denotes the desktop computer that controls all the instruments, and performs the calculations for the feedback orbit correction.